SCIENCE CHINA
Chemistry

•COMMUNICATIONS•

May 2022 Vol.65 No.5: 858–862
https://doi.org/10.1007/s11426-022-1211-5

Planet-satellite cage hybrids: covalent organic cages encircling metal organic cage

Chenjuan Yu[1,2†], Pan Yang[1†], Xinyuan Zhu[1] & Youfu Wang[1*]

[1]*School of Chemistry and Chemical Engineering, Frontiers Science Center for Transformative Molecules, Shanghai Jiao Tong University, Shanghai 200240, China;*
[2]*School of Materials Engineering, Shanghai University of Engineering Science, Shanghai 201620, China*

Received January 12, 2022; accepted February 10, 2022; published online April 2, 2022

As a rising type of precisely molecular nanoobjects, porous molecular cages, including covalent organic cages (COCs) and metal organic cages (MOCs), have attracted much more attention. It is fascinating to construct well-defined cage hybrids combining COCs and MOCs to further rich their types, properties, and applications. However, it is a big challenge due to the isotropy of the porous molecular cages. In this article, an anisotropic COC ligand based on aryl ether bonds and bearing one isophthalate moiety has been designed and synthesized. Then planet-satellite cage hybrids (PSCHs), MOC@COCs, have been constructed through the coordination of the anisotropic COC ligand and copper ions with or without the help of extra dicarboxylic ligands in an almost quantitative manner for the first time. Three PSCHs with one different topological MOC (heteroleptic bipolar, distorted cuboctahedral or homoleptic cuboctahedral) as the planet and different numbers of COCs (6, 12 or 24) as satellites are obtained. The structural and thermal properties of these PSCHs have also been studied. The obtained PSCHs exhibit discrete, uniform and stable structures, good solubility and strong film-forming property.

cage hybrid, planet-satellite, covalent organic cage, metal organic cage, giant molecule

Citation: Yu C, Yang P, Zhu X, Wang Y. Planet-satellite cage hybrids: covalent organic cages encircling metal organic cage. *Sci China Chem*, 2022, 65: 858–862, https://doi.org/10.1007/s11426-022-1211-5

There are vast precise objects with different scales and functions in nature, from atoms, molecules, biomacromolecules, viruses, bacteria, cells, organs to lives. Atomically precise nanoobjects will help us to understand the evolution from basic atomic or molecular scale to macroscopic world. The construction of atomically precise nanoobjects with well-defined chemical and spatial structures is a fundamental and important topic in chemical science. After the strenuous efforts by numerous scientists, a variety of well-defined nanoobjects have been synthesized and their properties and applications have also been deeply studied, such as nanocarbons [1,2], dendrimers [3,4], atomic clusters [5–7], and porous molecular cages. These manmade precise nanoobjects have promoted the deep interpretations of basic scientific processes and principles and then affected our lives in many aspects.

As a rising type of atomically precise nanoobject, porous molecular cages have attracted more and more attention during the last two decades. Porous molecular cages are typical polyhedra constructed from building blocks through reversibly chemical bonds. Based on the interactions between building blocks, porous molecular cages are mainly divided into covalent/porous organic cages (COCs or POCs) [8–10] and metal organic cages/polyhedrons (MOCs or MOPs) [11–13]. Due to the diverse building blocks and interaction modes, the porosities, properties and functions of porous molecular cages can be adjusted to meet the different needs of various applications, such as adsorption, separation,

†These authors contributed equally to this work.
*Corresponding author (email: wyfown@sjtu.edu.cn)

catalysis, biomedicine, energy storage and conversion. To further expand their research scopes, the structural complexity of porous molecular cages is continuously improved, such as giant cages [14,15], interlocked cages [16], cage oligomers [17,18], cage frameworks (covalent organic frameworks, COFs [19–22] and metal organic frameworks, MOFs [23–25]), porous polymers [26,27] and gels [28,29].

Due to the fascinating structures, properties and applications of these porous molecular cages, the giant cage hybrids with well-defined chemical and spatial structures combining these two kinds of porous molecular cages will give full play to their respective advantages [30–33]. Due to the structural isotropy of most of the porous molecular cages, it is a challenge to construct giant cage hybrids in an effective way. In this article, we constructed planet-satellite cage hybrids (PSCHs) through the coordination between anisotropic COCs with copper ions for the first time. We designed and synthesized a stable and soluble COC ligand based on aryl ether bonds and bearing one isophthalate moiety. Then, through the coordination-driven self-assembly of the anisotropic COC ligand and copper ions with or without the help of extra dicarboxylic ligands, three PSCHs with one different topological MOC (heteroleptic bipolar, distorted cuboctahedral or homoleptic cuboctahedral) as the planet and different numbers of COCs (6, 12 or 24) as satellites were obtained in an almost quantitative manner, donated as PSCH-A, PSCH-B and PSCH-C, respectively (Figure 1). The COC satellites are flexibly but robustly attached to the MOC planet. The structural and thermal properties of these PSCHs were studied. These PSCHs exhibited discrete, uniform and stable structures, excellent solubility in common solvents and film-forming properties.

The anisotropic COC ligand was synthesized *via* functionalization of shape-persistent bis(tetraoxacalix[2]arene [2]-triazine) cage with D_{3h} symmetry and three evenly distributed reactive sites (details in the Experimental section, Scheme S1, Supporting Information online) [18,34,35]. All the synthesized compounds were structurally confirmed by nuclear magnetic resonance (NMR) and mass spectroscopy (Figures S1–S6, Supporting Information online). The obtained COC ligand bearing one isophthalate moiety is stable and soluble due to the aryl ether bonds within the COC skeleton and the multiple alkyl chains on the COC surface. The isophthalate moiety within the COC ligand can construct various cuboctahedral MOCs through coordination with diverse $M_2(COO^-)_4$ paddlewheel units (M = copper, molybdenum, rhodium, ruthenium, chromium) and much more topological MOCs with the help of extra dicarboxylic ligands [36–39]. Here, two dicarboxylic ligands with bridging angles of 60° for biphenyl-3,3′-dicarboxylic (L) and 120° for naphthalene-2,7-dicarboxylic (L′), were utilized as extra ligands to construct different interior MOC planets. After mixing the COC ligand with or without the extra ligands and an equimolar

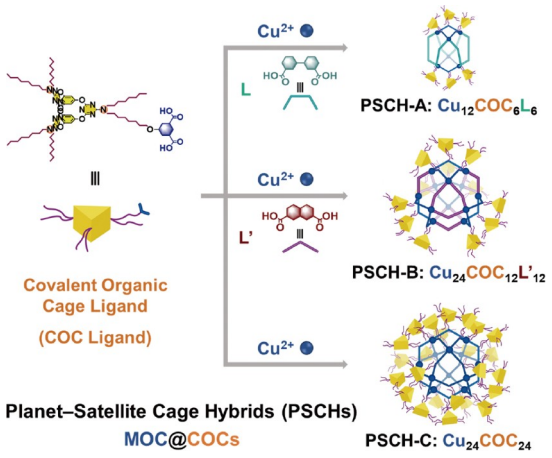

Figure 1 The construction of PSCHs through coordination between anisotropic COC ligand bearing one isophthalate moiety and copper ions with or without the help of extra dicarboxylic ligands. These PSCHs contain one different topological MOC as the planet and 6, 12 or 24 COCs as satellites for PSCH-A, PSCH-B and PSCH-C, respectively (color online).

amount of copper(II) acetate monohydrate in tetrahydrofuran (THF), the PSCHs with one different topological MOC as the planet and 6, 12 or 24 COCs as satellites were constructed effectively through the coordination-driven self-assembly. Through self-sorting procession [39–41], the heteroleptic bipolar PSCH-A with the formula of $Cu_{12}COC_6L_6$, the distorted cuboctahedral PSCH-B with the formula of $Cu_{24}COC_{12}L'_{12}$ and the homoleptic cuboctahedral PSCH-C with the formula of $Cu_{24}COC_{24}$ were obtained through forming the paddlewheel $Cu_2(COO^-)_4$ connected units. These PSCHs can be isolated as blue powders in also a quantitative manner (yields > 92%) through precipitation in methanol, centrifugation and dry. The obtained PSCHs powders can be redissolved in many common solvents due to a large number of alkyl chains on the periphery, such as THF, chloroform, dichloromethane, diethyl ether, toluene, n-hexane, acetone, and dimethylformamide (Figure S7).

The Fourier transform infrared (FTIR) spectroscopy was used to confirm the structures of the COC ligand and assembled PSCHs (Figure S8). Using PSCH-C as an example, the spectrum of PSCH-C is almost the same with that of COC ligand. However, the characteristic bands of triazine ring within COC ligand at 810, 1,590 and 1,614 cm^{-1} shift to 809, 1,594 and 1,641 cm^{-1} within PSCH-C. The characteristic band of isophthalate within COC ligand at 1,728 cm^{-1} disappeared after the formation of PSCH-C indicating the coordination between isophthalate and copper ions. Both PSCH-A and PSCH-B show the characteristic bands within the related ligands. There are also band shifts of triazine ring and band disappearances of carboxylic within COC ligand and L or L′ for PSCH-A and PSCH-B, respectively.

Due to the multicomponent features of PSCH-A and PSCH-B, the PSCH-C was chosen to run NMR to study the coordination behaviors. From the ^1H nuclear magnetic re-

sonance (NMR) spectra of the COC ligand and PSCH-C in deuterated chloroform (Figure S9), the aromatic peaks around 6.56 ppm corresponding to the cage moiety within the COC ligand are maintained and broaden in the assembled PSCH-C. However, the aromatic peaks of 8.40 and 7.82 ppm corresponding to the isophthalate moiety within COC ligand shift to the lower field and broaden in the assembled PSCH-C due to the coordination of isophthalate with copper. The peak of methylene group close to isophthalate moiety at 4.06 ppm also shifts to lower field and broadens due to the coordination. The NMR spectra also confirm the coordination between the anisotropic COC ligand and copper ions.

A small aliquot of the coordination reaction solution was taken and diluted with THF to run the size exclusion chromatography (SEC) analysis. All the SEC plots of the COC ligand and PSCHs in THF showed a single sharp peak at t = 19.1, 17.8, 17.1 and 17.0 min, respectively (Figure 2a). The disappearance of COC ligand signal in SEC plots of the PSCHs also indicates the high efficiency during the coordination assembly. The shorter elution times for the formed PSCHs than the pristine COC ligand imply the larger hydrodynamic volumes of the assembled PSCHs than the COC ligand. The molecular weights of the COC ligand and PSCHs calculated from SEC plots were about 2,800, 13,200, 25,500 and 29,500 g/mol with the exceptionally narrow polydispersity of 1.06, 1.08, 1.02 and 1.02, respectively (relative to polymethyl methacrylate standards) (Table 1). The increased molecular weights indicate the increased hydrodynamic volumes from PSCH-A to PSCH-C consistent with the size changes of the envisaged structures. The difference of the obtained molecular weights from SEC between PSCH-B and PSCH-C is much smaller than the theoretical values due to their similar sizes. This indicates the formation of discrete, uniform and stable PSCHs in an effective way.

The matrix-assisted laser desorption ionization time-of-flight (MALDI-TOF) mass spectrometry was used to estimate the molecular weights of the obtained PSCHs. Using trans-2-[3-(4-*tert*-butylphenyl)-2-methyl-2-propenylidene]malononitrile (DCTB) as the matrix, the obtained PSCHs exhibit prominent peaks at m/z = 10,538, 21,024 and 34,565 corresponding to the molecular weights of ionized PSCHs species (theoretical molecular weights of these PSCHs: 10,468.46, 20,624.73 and 34,602.51 Da; Figures 2b and S10, Table 1). The MALDI-TOF results further indicate that the expected PSCHs with one different topological MOC as the planet and different numbers of COCs as satellites were formed.

The transmission electron microscopy (TEM) and atomic force microscopy (AFM) were applied to observe the morphologies and sizes of the obtained PSCHs. A drop of the PSCHs solution in THF (about 0.2 mg/mL) was placed on a copper grid to run TEM experiments. The observed PSCHs are discretely and compactly spherical nanoobjects with uniform diameters about 2.5, 5.4 and 5.5 nm for PSCH-A,

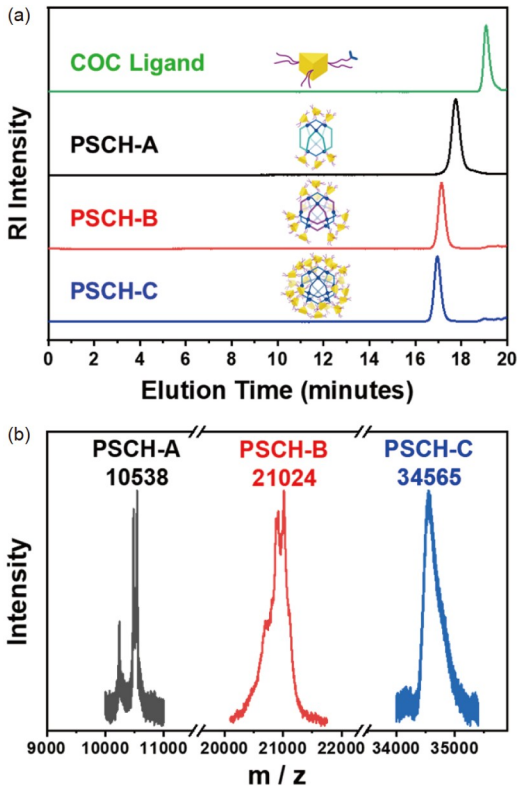

Figure 2 (a) The SEC plots of the COC ligand and the PSCHs in THF inserted with the schematic structures. (b) The MALDI-TOF mass spectra of the PSCHs with DCTB as the matrix (color online).

PSCH-B and PSCH-C, respectively (Figure S11). The quite close sizes of PSCH-B and PSCH-C are consistent with the SEC results. For AFM experiments, we prepared thin-film samples by spin-casting a highly diluted chloroform solution of PSCHs (10 ng/mL) on a mica substrate (Figure 3). The observed PSCH-A and PSCH-C also show uniformly, discretely and compactly spherical morphologies on the substrate, indicating the structural rigidness of these two PSCH systems. The PSCH-B shows so-called "sunny-side up egg" morphology due to the lower density of the peripheral COC satellites [42,43]. The heights of these PSCHs were about 2.2, 5.0 and 6.3 nm for PSCH-A, PSCH-B and PSCH-C, respectively. Considering the sizes of the cuboctahedral MOC core about 3.4 nm [44] and of the COC about 1.0 nm [34], the COC satellites should slightly tightly surround on the cuboctahedral MOC planet for PSCH-C. That is why the height of PSCH-C is slightly larger than that of PSCH-B and these two PSCH systems exhibit different morphologies in AFM images. It was observed that the diameters of each PSCHs are quite uniform, fitting well with the narrow polydispersity as determined by SEC and the single prominent peak from MALDI-TOF result.

The sizes of the COC ligand and PSCHs were also estimated by dynamic light scattering (DLS) in THF (Table 1 and Figure S12). The average sizes of the COC ligand and PSCHs are about 1.0, 5.1, 9.1 and 12.8 nm with narrow polydispersity

Table 1 The molecular weights and sizes of the COC ligand and the PSCHs

Entry	$M_{n,\ theoretical}$ (g/mol)	$M_{n,\ SEC}$ (g/mol)	$Đ_{SEC}$	$M_{n,\ Maldi}$ (g/mol)	$Size_{DLS}$ (nm)	$Đ_{DLS}$
COC ligand	1380.86	2800	1.06	1381.85	1.0	0.23
PSCH-A	10468.46	13200	1.08	10538	5.1	0.19
PSCH-B	20624.73	25500	1.02	21024	9.1	0.21
PSCH-C	34602.51	29500	1.02	34565	12.8	0.21

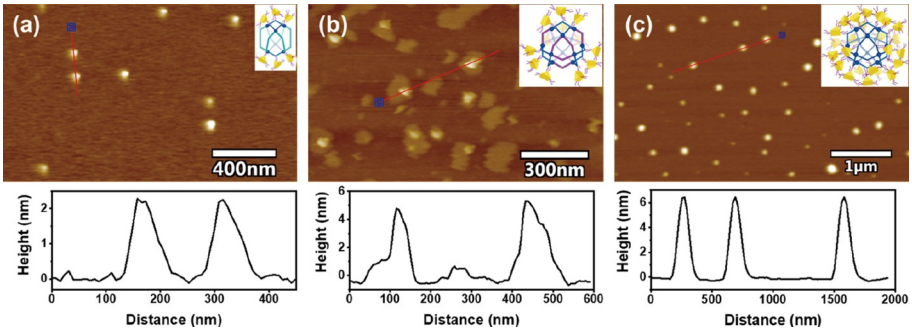

Figure 3 The AFM images and height analysis along the red line of the PSCHs. (a) PSCH-A, (b) PSCH-B and (c) PSCH-C with scale bars of 400 nm, 300 nm and 1 μm, respectively (color online).

around 0.20, which are slightly larger than the diameters from TEM and AFM maybe due to the solvation effect and peripheral alkyl chains. The tendency of the hydrodynamic sizes is consistent with the results from SEC.

Thermogravimetric analysis (TGA) was applied to assess the general thermal properties of the obtained PSCHs. From TGA plots of the COC ligand and PSCHs (Figure S13) under air flow at a heating rate of 10 °C/min, the COC ligand will completely decompose at 700 °C with two stages corresponding to the flexible alkyl chains and rigid COC core. The PSCHs are thermally stable up to 300 °C and then decompose gradually with stable mass residues of 11.5 wt%, 10.4 wt% and 6.4 wt%, respectively. The mass residues of these PSCHs should be cupric oxide with theoretical values of 9.1 wt%, 9.2 wt% and 5.5 wt% which is well matched with the tested values. This further indicated the formation of the expected cage hybrid structures.

The small angle X-ray scattering (SAXS) measurements were conducted to gain insight into the nanostructures of the PSCHs. The as-prepared PSCHs, which were isolated as blue crystalline materials by precipitation from methanol and vacuum dry (Figure S7), formed a very short-range order as indicated by the appearance of one sharp peak and one or two weak peaks (Figure 4a). The distances between stacking PSCHs and COCs are donated as d_1 and d_2, respectively (Figure 4b). The heteroleptic bipolar PSCH-A has two peaks around Q = 0.148 and 0.385 Å^{-1}, corresponding to the d_1 of 4.25 nm and d_2 of 1.63 nm. The distorted cuboctahedral PSCH-B has two peaks around Q = 0.140 and 0.364 Å^{-1}, corresponding to the d_1 of 4.48 nm and d_2 of 1.73 nm. The homoleptic cuboctahedral PSCH-C has two peaks around Q = 0.135 and 0.398 Å^{-1}, corresponding to the d_1 of 4.65 nm and d_2 of 1.58 nm. The COC-COC distance in PSCH-C is smaller than that in PSCH-B, indicating the closer stacking of COCs on PSCH-C consistent with their morphology differences in AFM images. The distances between PSCHs are much smaller than their sizes in solution, which indicates an interpenetration of the COC ligands within the isolated PSCHs powders.

Due to the porosity of the COCs and MOCs within PSCHs, the porous characters of these PSCHs were evaluated by the N_2 gas sorption-desorption isotherm at 77 K. These PSCHs are almost nonporous. The exact COC is nonporous, proved by many literatures [19]. Most copper-isophthalate MOCs are nonporous especially when large groups on the periphery. On the other hand, both the closely stacked structures and the filling of extensive flexible alkyl chains will further decrease the porosity of these PSCHs, consistent with the interpenetration behavior of these PSCHs from the SAXS test.

The solution-processable nature and good solubility of these PSCHs prompted us to prepare uniform self-standing films with well-organized arrangements *via* a solution-based procedure. The THF solution of PSCH-C was layered on dimethylacetamide. A blue-colored film that was robust enough to be picked up with tweezers (Figure S14) was obtained after the slow evaporation of THF at room temperature.

In summary, an anisotropic COC ligand based on aryl ether bonds and bearing one isophthalate moiety was designed and synthesized. Then planet-satellite cage hybrids combining MOC and COC were fabricated through the coordination between the anisotropic COC ligand and copper ions with or without the help of extra dicarboxylic ligands in high efficiency for the first time. Three planet-satellite cage hybrids

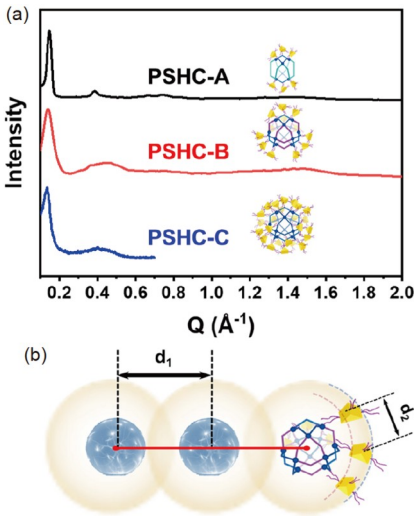

Figure 4 (a) The SAXS plots of the PSCHs and (b) the schematic diagram of PSCH stacking structure and related distances (color online).

with one different topological MOC as the planet and different numbers of COCs as satellites were constructed and structurally confirmed. These planet-satellite cage hybrids exhibit discrete, uniform and stable structures. The high solubility and stability of these cage hybrids promote the film-forming properties through solution procession. The cage hybrids build a bridge between MOC and COC and a bridge between molecular cages and frameworks (MOFs, COFs). The developed effective strategy to construct cage hybrids can further expand the types of cage-based nanoobjects with different metals, connection modes and morphologies and then broaden related properties and applications.

Acknowledgements This work was supported by the National Natural Science Foundation of China (21805130). The authors thank the support from Instrumental Analysis Center of Shanghai Jiao Tong University.

Conflict of interest The authors declare no conflict of interest.

Supporting information The supporting information is available online at http://chem.scichina.com and http://link.springer.com/journal/11426. The supporting materials are published as submitted, without typesetting or editing. The responsibility for scientific accuracy and content remains entirely with the authors.

1 Segawa Y, Ito H, Itami K. *Nat Rev Mater*, 2016, 1: 15002
2 Guo QH, Qiu Y, Wang MX, Fraser Stoddart J. *Nat Chem*, 2021, 13: 402–419
3 Astruc D, Boisselier E, Ornelas C. *Chem Rev*, 2010, 110: 1857–1959
4 Bronstein LM, Shifrina ZB. *Chem Rev*, 2011, 111: 5301–5344
5 Jena P, Sun Q. *Chem Rev*, 2018, 118: 5755–5870
6 Kang X, Li Y, Zhu M, Jin R. *Chem Soc Rev*, 2020, 49: 6443–6514
7 Khatun E, Pradeep T. *ACS Omega*, 2021, 6: 1–16
8 Zhang G, Mastalerz M. *Chem Soc Rev*, 2014, 43: 1934–1947
9 Hasell T, Cooper AI. *Nat Rev Mater*, 2016, 1: 16053
10 Mastalerz M. *Acc Chem Res*, 2018, 51: 2411–2422
11 Vardhan H, Yusubov M, Verpoort F. *Coord Chem Rev*, 2016, 306: 171–194
12 Lee S, Jeong H, Nam D, Lah MS, Choe W. *Chem Soc Rev*, 2021, 50: 528–555
13 Zhang D, Ronson TK, Zou YQ, Nitschke JR. *Nat Rev Chem*, 2021, 5: 168–182
14 Koo J, Kim I, Kim Y, Cho D, Hwang IC, Mukhopadhyay RD, Song H, Ko YH, Dhamija A, Lee H, Hwang W, Kim S, Baik MH, Kim K. *Chem*, 2020, 6: 3374–3384
15 Fujita D, Ueda Y, Sato S, Mizuno N, Kumasaka T, Fujita M. *Nature*, 2016, 540: 563–566
16 Frank M, Johnstone MD, Clever GH. *Chem Eur J*, 2016, 22: 14104–14125
17 Greenaway RL, Santolini V, Szczypiński FT, Bennison MJ, Little MA, Marsh A, Jelfs KE, Cooper AI. *Chem Eur J*, 2020, 26: 3718–3722
18 Yu C, Yang Y, Wang Y. *New J Chem*, 2021, 45: 22049–22052
19 Ma JX, Li J, Chen YF, Ning R, Ao YF, Liu JM, Sun J, Wang DX, Wang QQ. *J Am Chem Soc*, 2019, 141: 3843–3848
20 Shan Z, Wu X, Xu B, Hong YL, Wu M, Wang Y, Nishiyama Y, Zhu J, Horike S, Kitagawa S, Zhang G. *J Am Chem Soc*, 2020, 142: 21279–21284
21 Zhu Q, Wang X, Clowes R, Cui P, Chen L, Little MA, Cooper AI. *J Am Chem Soc*, 2020, 142: 16842–16848
22 Ji C, Su K, Wang W, Chang J, El-Sayed ESM, Zhang L, Yuan D. *CCS Chem*, 2021, 3: 3094–3104
23 Perry IV JJ, Perman JA, Zaworotko MJ. *Chem Soc Rev*, 2009, 38: 1400–1417
24 Chen L, Chen Q, Wu M, Jiang F, Hong M. *Acc Chem Res*, 2015, 48: 201–210
25 Grancha T, Carné-Sánchez A, Zarekarizi F, Hernández-López L, Albalad J, Khobotov A, Guillerm V, Morsali A, Juanhuix J, Gándara F, Imaz I, Maspoch D. *Angew Chem Int Ed*, 2021, 60: 5729–5733
26 Carne-Sanchez A, Craig GA, Larpent P, et al. *Nat Commun*, 2018, 9: 2506
27 Giri A, Sahoo A, Dutta TK, Patra A. *ACS Omega*, 2020, 5: 28413–28424
28 Foster JA, Parker RM, Belenguer AM, Kishi N, Sutton S, Abell C, Nitschke JR. *J Am Chem Soc*, 2015, 137: 9722–9729
29 Jahović I, Zou YQ, Adorinni S, Nitschke JR, Marchesan S. *Matter*, 2021, 4: 2123–2140
30 Sun QF, Murase T, Sato S, Fujita M. *Angew Chem Int Ed*, 2011, 50: 10318–10321
31 Bhat IA, Samanta D, Mukherjee PS. *J Am Chem Soc*, 2015, 137: 9497–9502
32 Sun B, Wang M, Lou Z, Huang M, Xu C, Li X, Chen LJ, Yu Y, Davis GL, Xu B, Yang HB, Li X. *J Am Chem Soc*, 2015, 137: 1556–1564
33 Yin JF, Zheng Z, Yang J, Liu Y, Cai L, Guo QY, Li M, Li X, Sun TL, Liu GX, Huang C, Cheng SZD, Russell TP, Yin P. *Angew Chem Int Ed*, 2021, 60: 4894–4900
34 Wang DX, Wang QQ, Han Y, Wang Y, Huang ZT, Wang MX. *Chem Eur J*, 2010, 16: 13053–13057
35 Wang QQ, Luo N, Wang XD, Ao YF, Chen YF, Liu JM, Su CY, Wang DX, Wang MX. *J Am Chem Soc*, 2017, 139: 635–638
36 Li JR, Yakovenko AA, Lu W, Timmons DJ, Zhuang W, Yuan D, Zhou HC. *J Am Chem Soc*, 2010, 132: 17599–17610
37 Ahmad N, Chughtai AH, Younus HA, Verpoort F. *Coord Chem Rev*, 2014, 280: 1–27
38 Hosono N, Kitagawa S. *Acc Chem Res*, 2018, 51: 2437–2446
39 Li JR, Zhou HC. *Nat Chem*, 2010, 2: 893–898
40 Zhang D, Ronson TK, Nitschke JR. *Acc Chem Res*, 2018, 51: 2423–2436
41 Yu H, Li J, Shan C, Lu T, Jiang X, Shi J, Wojtas L, Zhang H, Wang M. *Angew Chem Int Ed*, 2021, 60: 26523–26527
42 Hosono N, Gochomori M, Matsuda R, Sato H, Kitagawa S. *J Am Chem Soc*, 2016, 138: 6525–6531
43 Hosono N, Omoto K, Kitagawa S. *Chem Commun*, 2017, 53: 8180–8183
44 Eddaoudi M, Kim J, Wachter JB, Chae HK, O'Keeffe M, Yaghi OM. *J Am Chem Soc*, 2001, 123: 4368–4369